Supporting Information

Underwater unidirectional cellular fluidics

Mingzhu Xie[1], Huigao Duan[1], Ping Cheng[2], Yongping Chen[3], Zhichao Dong[4]*, Zhaolong Wang[1]*

[1] College of Mechanical and Vehicle Engineering, Hunan University, Changsha 410082, PR China

[2] MOE Key Laboratory for Power Machinery and Engineering, School of Mechanical Engineering, Shanghai Jiao Tong University, Shanghai 200240, PR China

[3] Key Laboratory of Energy Thermal Conversion and Control of Ministry of Education, School of Energy and Environment, Southeast University, Nanjing 210096, PR China

[4] Key Laboratory of Bio-inspired Materials and Interface Sciences, Technical Institute of Physics and Chemistry, Chinese Academy of Sciences, Beijing 100190, PR China

*Corresponding authors. Emails: zhaolongwang@hnu.edu.cn(Z.W.); dongzhichao@mail.ipc.ac.cn (Z.D.)

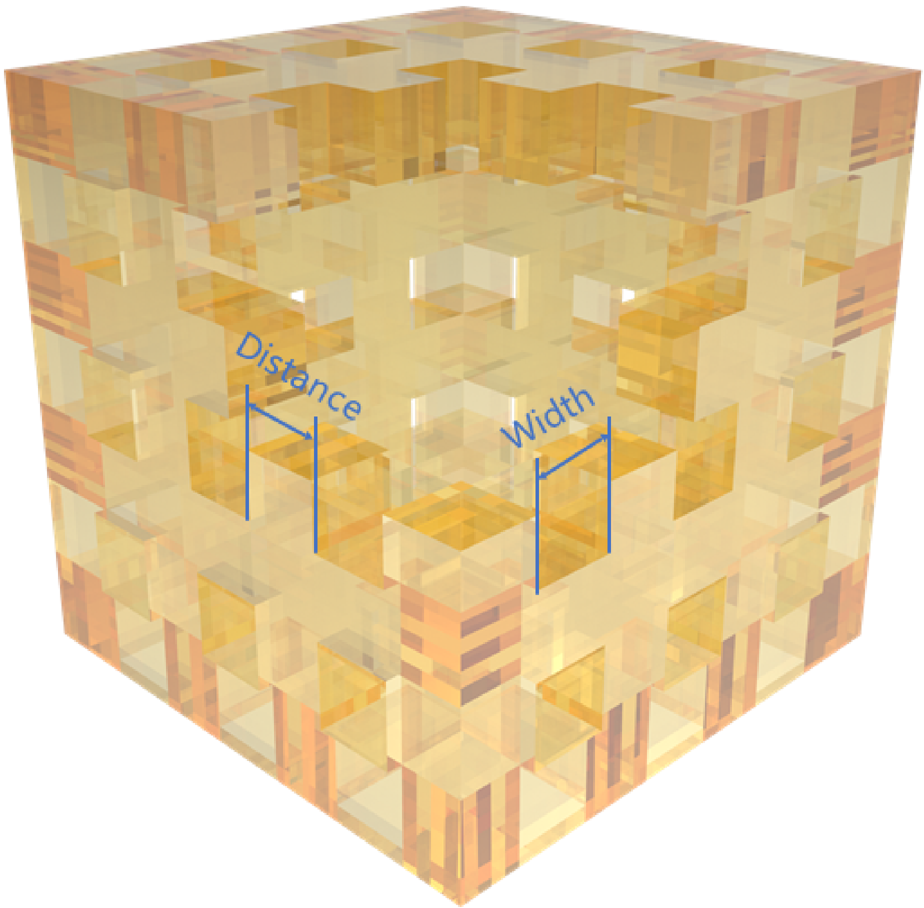

Figure S1. Schematic of a 3D printed bionic cell. The width of the holes and the distance between two adjacent holes are indicated.

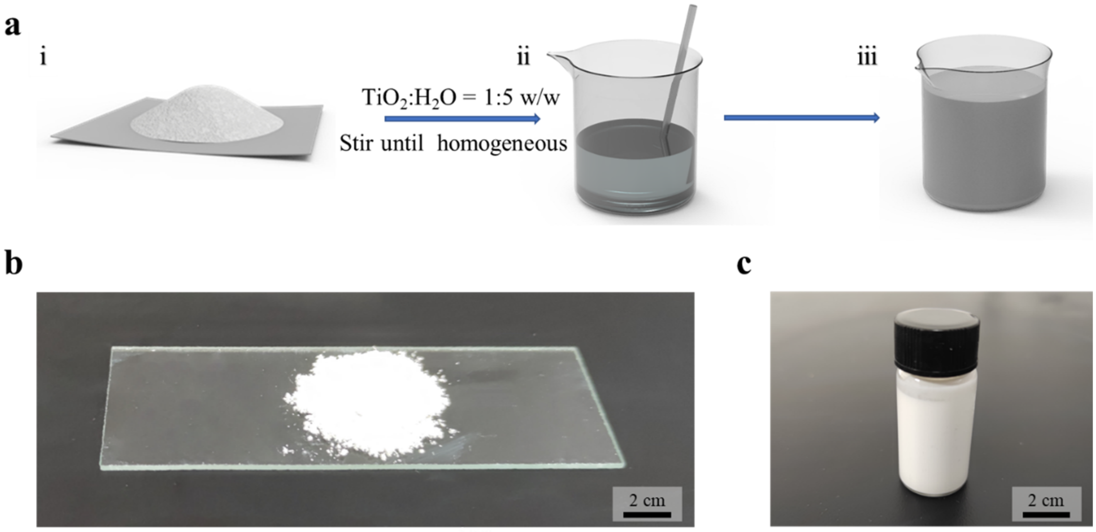

Figure S2. Preparation process of TiO_2 slurry. (a) A certain amount of TiO_2 nanoparticle powder was added into a beaker containing DI water, the weighting ratio of DI water and TiO_2 nanoparticle powder was 5:1. The mixture was stirred for 3 min to obtain a homogeneous medium, (b) TiO_2 nanoparticles, (c) TiO_2 nanoparticle sizing agent.

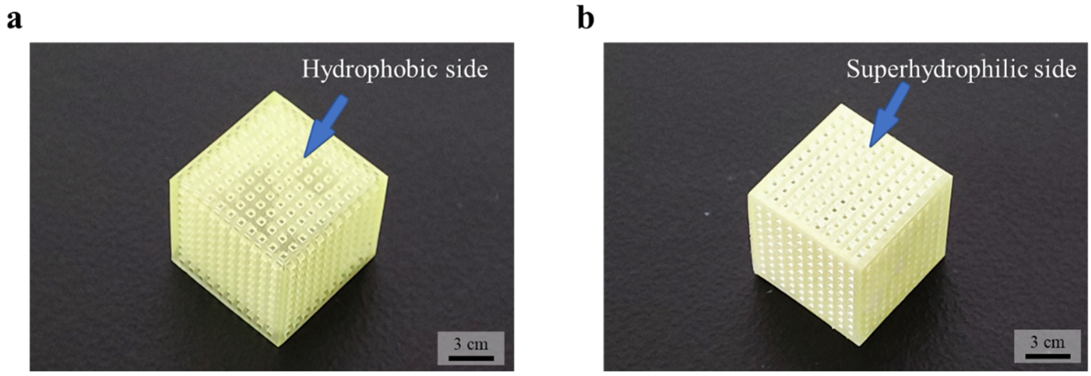

Figure S3. A 3D printed bionic open cell with rectangular holes. (a) A 3D printed bionic open cell with an untreated outer surface. (b) The outer surface of a 3D printed bionic open cell had been treated with TiO_2 nanoparticle slurry.

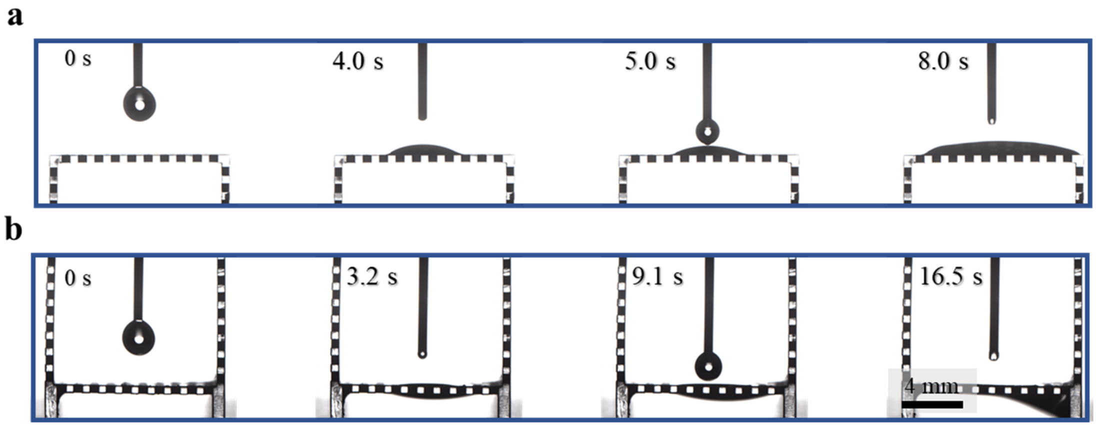

Figure S4. Unidirectional fluidics of our bionic open cell. (a) A DI water droplet spread on the surface if it was dripped on the superhydrophilic surface. (b) A DI water droplet penetrated to the superhydrophilic surface within a few seconds if it was dripped on the hydrophobic surface.

a b

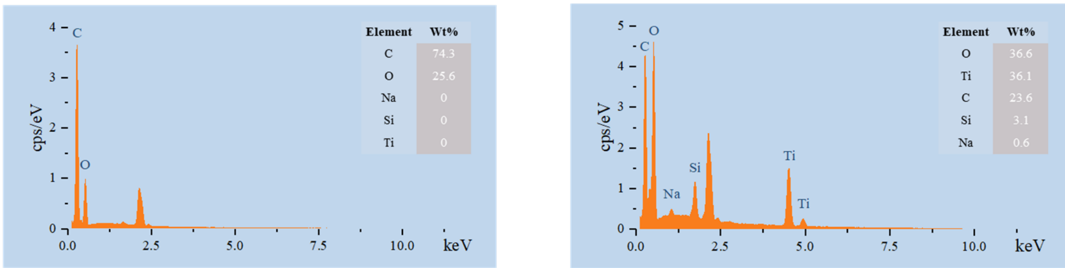

Figure S5. The energy spectrum diagram (EDS) for the inside and outside surfaces of our bionic cell. (a) There was only carbon and oxygen on the original membrane, which came from the photo-curable resin. (b) There was a large amount of titanium on the surface of a membrane treated with TiO_2 nanoparticle slurry.

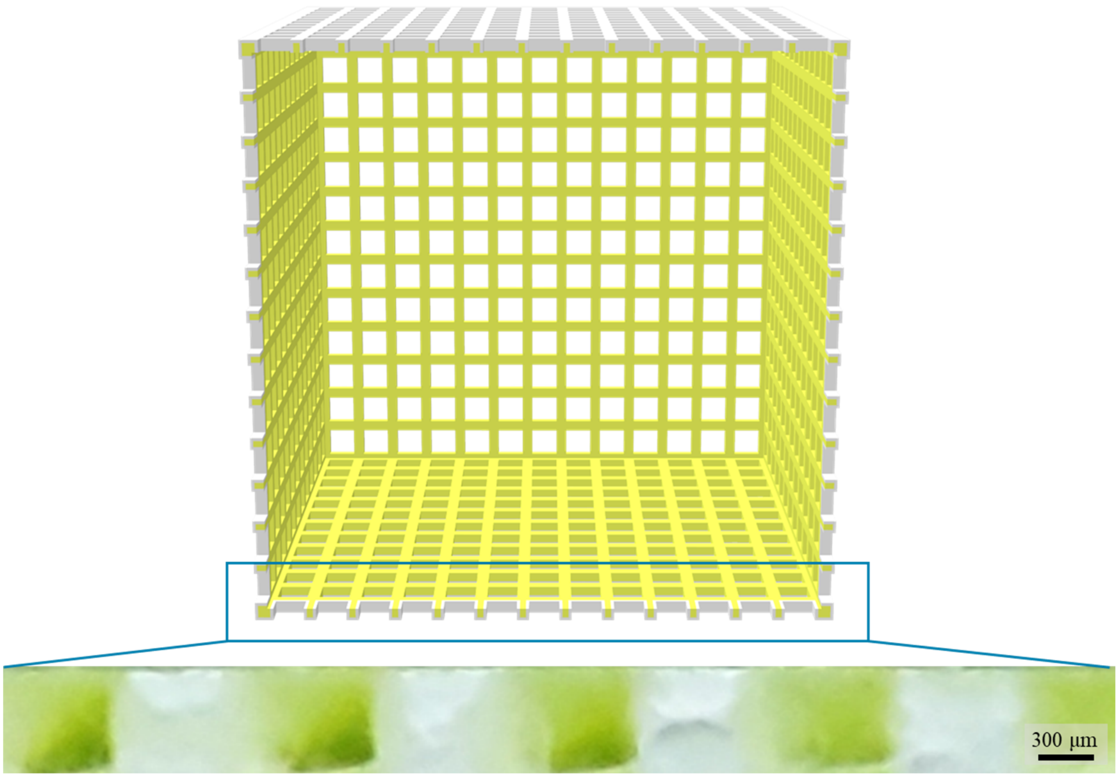

Figure S6. Image of the bionic cell cross section. The whole holes were covered by TiO_2 nanoparticles.

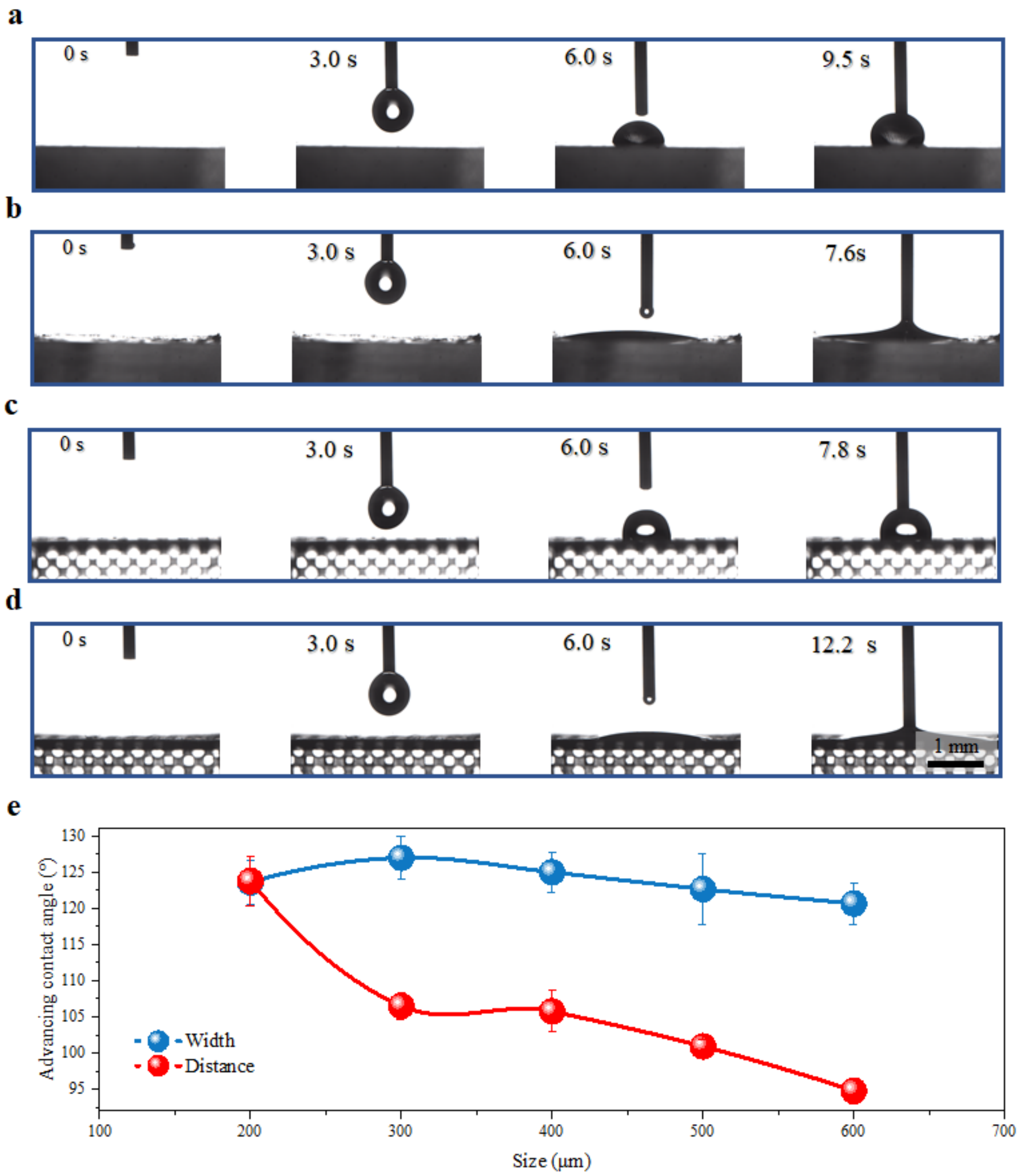

Figure S7. Advancing contact angles of different surfaces. (a) The advancing CA of an untreated flat. (b) The advancing CA of a flat treated with TiO_2 nanoparticle slurry. (c) The advancing CA of an untreated bionic open cell. (d) The advancing CA of a bionic open cell treated with TiO_2 nanoparticle slurry. (e) As the width of the holes increased, the advancing CA rose and then fell, the bionic membrane with holes' width of 300 μm had the largest advancing CA. Moreover, the advancing CA decreased with the increasing of the distance between two adjacent holes. The distance between two adjacent holes with different widths of holes is 400 μm and the width of holes with different the distances between two adjacent holes is 400 μm.

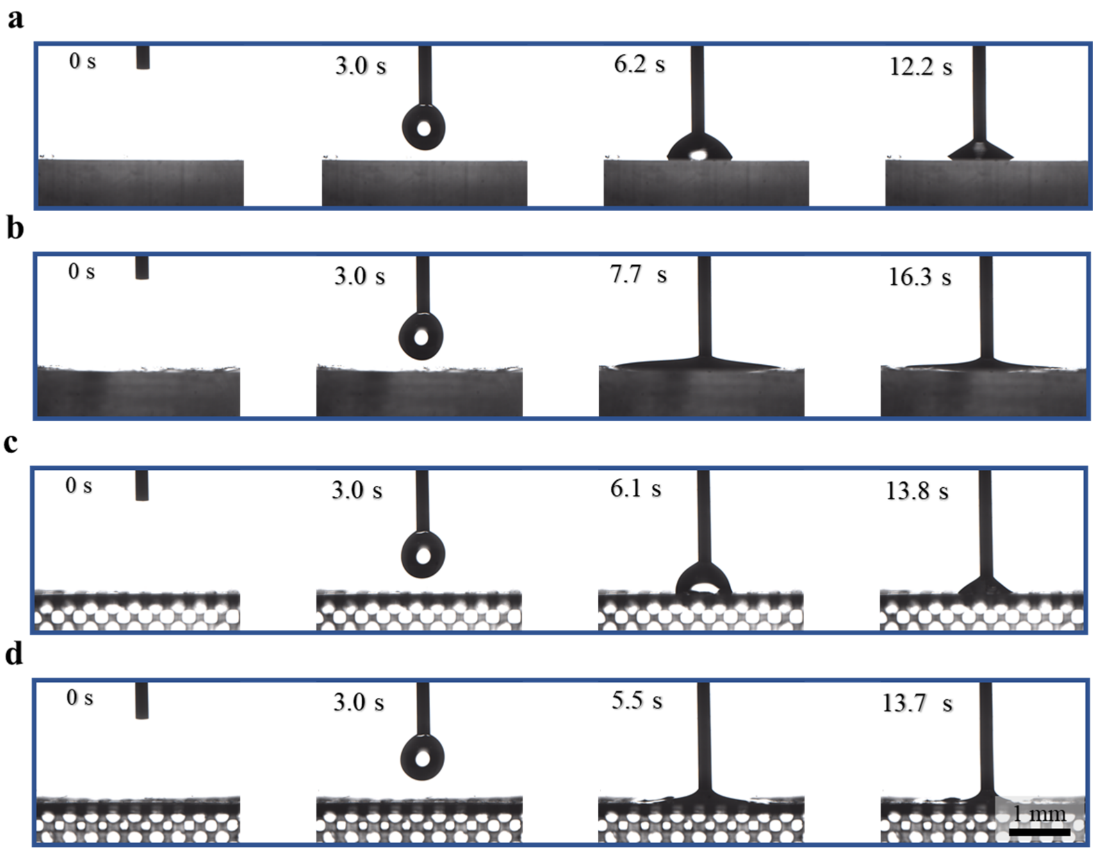

Figure S8. Receding CA of different surfaces. (a) The receding CA of an untreated flat. (b) The receding CA of a flat treated with TiO_2 nanoparticle slurry, (c) The receding CA of an untreated bionic open cell. (d) The receding CA of a bionic open cell treated with TiO_2 nanoparticle slurry.

Theoretical analysis of the Laplace pressure for liquid unidirectional penetration process

For the bending liquid surface, the Laplace pressure is given by

$$\Delta p = \gamma(\frac{1}{R_1} + \frac{1}{R_2}) \tag{S1}$$

where γ is the solid-liquid surface tension, R_1, R_2 are the curvature radius of any two orthogonal to a point on the surface subject to additional pressure Δp. When the curvature is always, $R_1 = R_2 = R$, for the system considered here, $R = D/(2\sin\theta)$, with D being the width of the hole and θ being the contact angle. Thus, we have

$$p_{in} - p_{out} = \Delta p = \frac{4\gamma \sin\theta}{\mathrm{D}} \tag{S2}$$

where p_{out} is environmental pressure, p_{in} is the pressure inside the bionic cell. Now we can analyze the dynamic process of the liquid unidirectional penetration as shown in Figure S8, where Figure S9a responds to the situation of the advancing contact angle $\theta_a \leq 90°$, while Figure S9b responds to the situation with the advancing contact angle $\theta_a > 90°$. Contact angle θ increases gradually with the solid-liquid contact line being fixed at the exit of the bionic cell. Liquid will not spill out of stomata until the advancing contact angle θ_a is reached. Then, the solid-liquid contact line will shift outward from the exit of the hole and advances with a constant contact angle of θ_a on the outer surface.

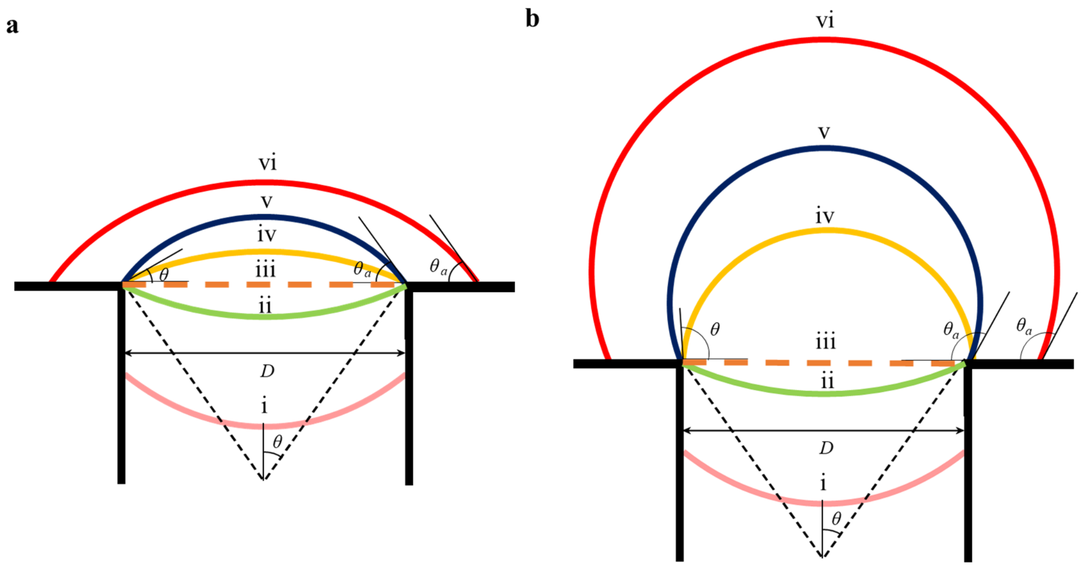

Figure S9. Contact lines of water outside of the holes. (a) $\theta_a \leq 90°$. (b) $\theta_a > 90°$

Figure S10 indicates the difference of the curvature radius during the dynamic process of liquid unidirectional penetration. As shown in Figure S10a, for the case with $\theta_a \leq 90°$, the surface curvature would increase with the increasing θ from iii to vi. During this process (iii to vi), the maximum Laplace pressure is obtained to be

$$\Delta p_{\max} = \frac{4\gamma \sin\theta_a}{\mathrm{D}} \tag{S3}$$

Beyond this pressure difference, the liquid will be driven out of the membrane.

For the situation with $\theta_a > 90°$ (Figure S10b), the curvature first increases with the increasing θ, reaches a maximum at $\theta = 90°$ and then decreases with further increase of θ. This implies that the process from iv to v is spontaneous. The maximum Laplace pressure during the process from iii to vi is obtained to be

$$\Delta p_{\max} = \frac{4\gamma}{\mathrm{D}} \tag{S4}$$

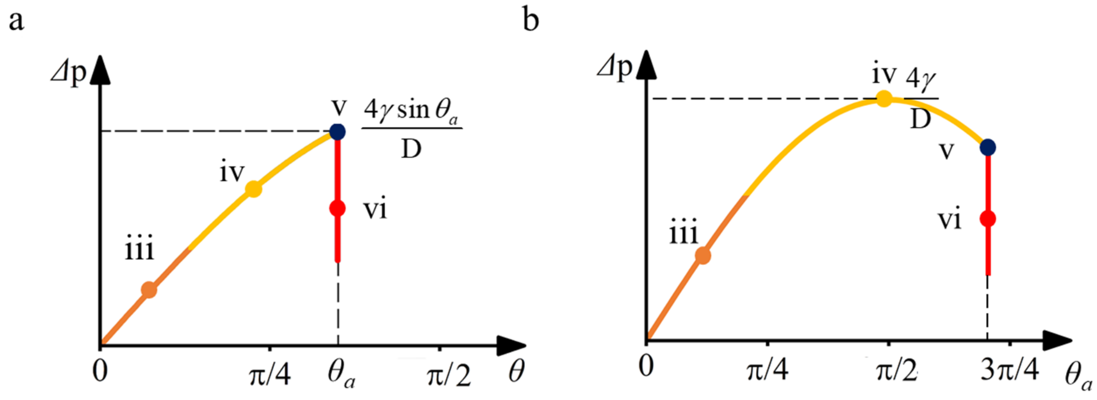

Figure S10. The change of the Laplace force during the penetration of liquid though a microhole. (a) $\theta_a \leq 90°$. (b) $\theta_a > 90°$.

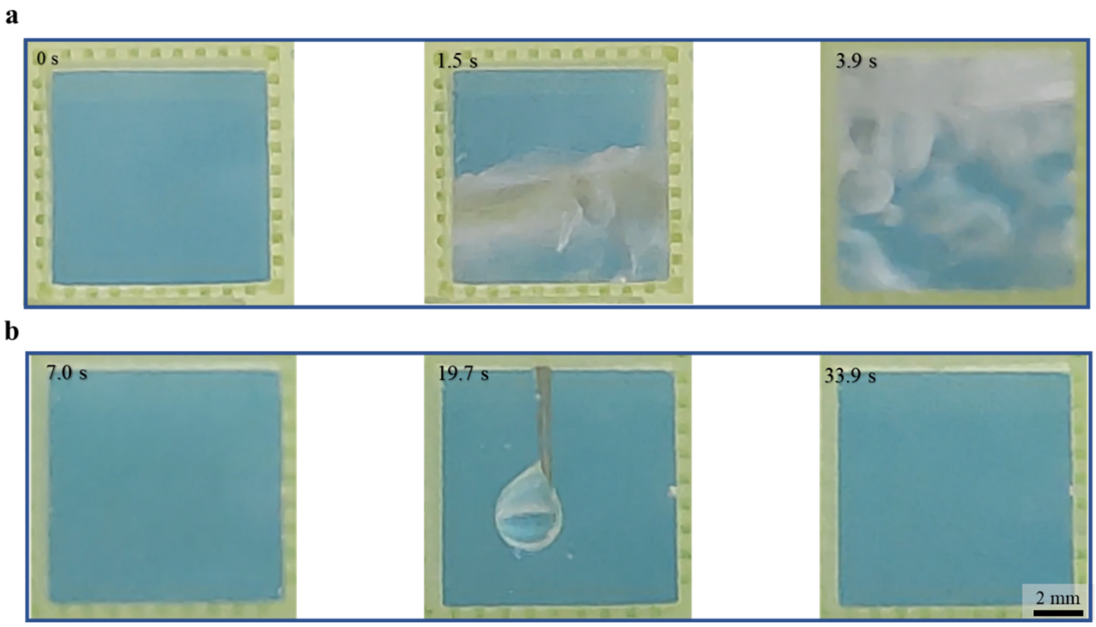

Figure S11. Unidirectional penetration of the bionic open cell underwater. (a) the bionic open cell was placed in a transparent water tank and water was continuously added to it until the bionic open cell was submerged into water. (b) Water was blocked outside of the bionic cell, when droplets are dripped on the inner cell wall through a needle, they would unidirectional penetrate out of the bionic cell.

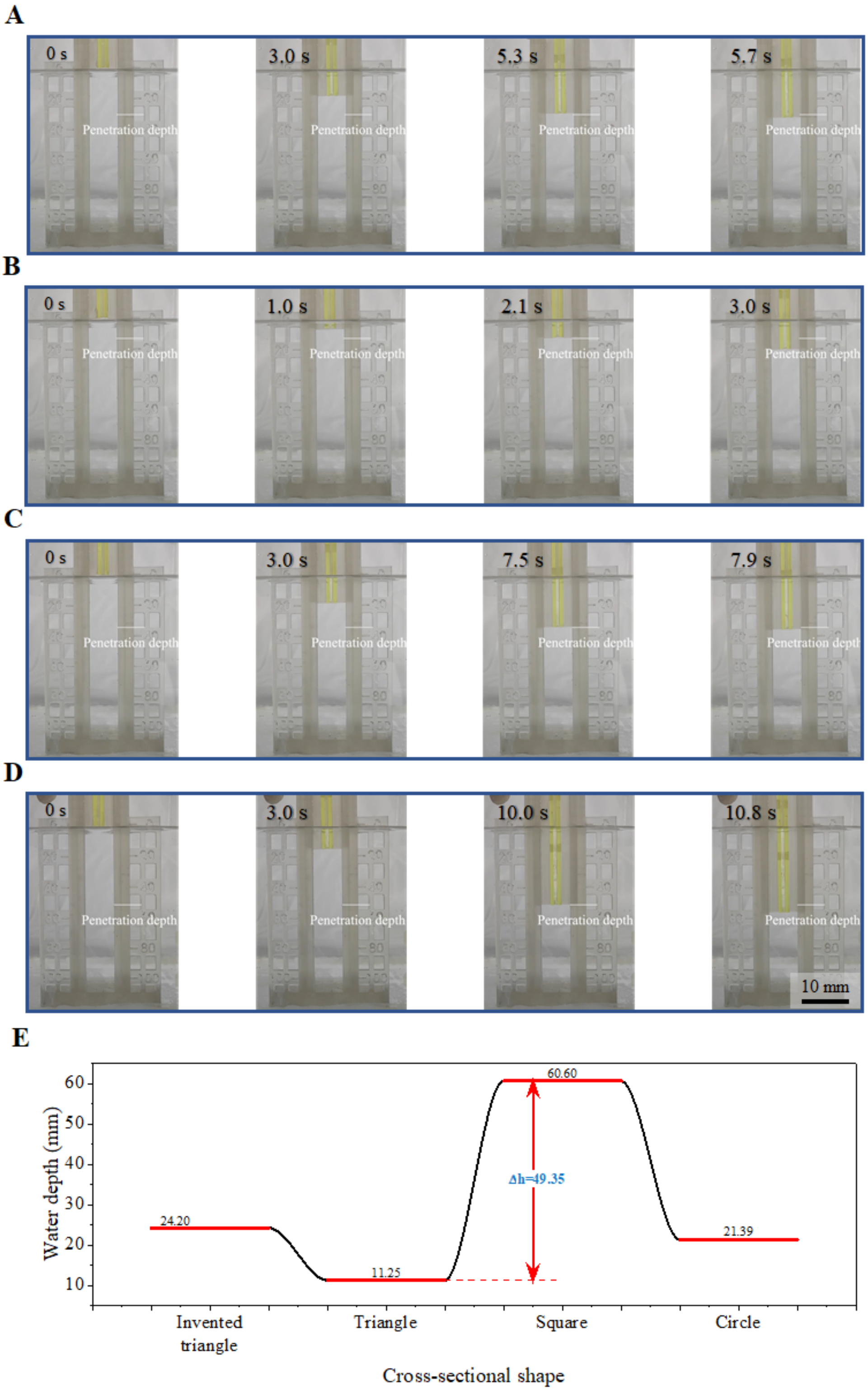

Figure S12. The influence of the hole's geometry on the capability to withstand water depth. (a) For a membrane with circular holes, the water depth the membrane could withstand was about 30 mm. (b) For a membrane with triangular holes, the water depth the membrane could withstand was about 15 mm. (c) W For a membrane with inverted triangular holes, the water depth the membrane could withstand was about 30 mm. (d) For a membrane with square holes, the water depth the membrane could withstand was about 55 mm. (e) The comparison of the water depth the membrane could withstand for different geometric holes. A membrane with square holes exhibited the best performance, while the one with triangular holes presented the worst performance.

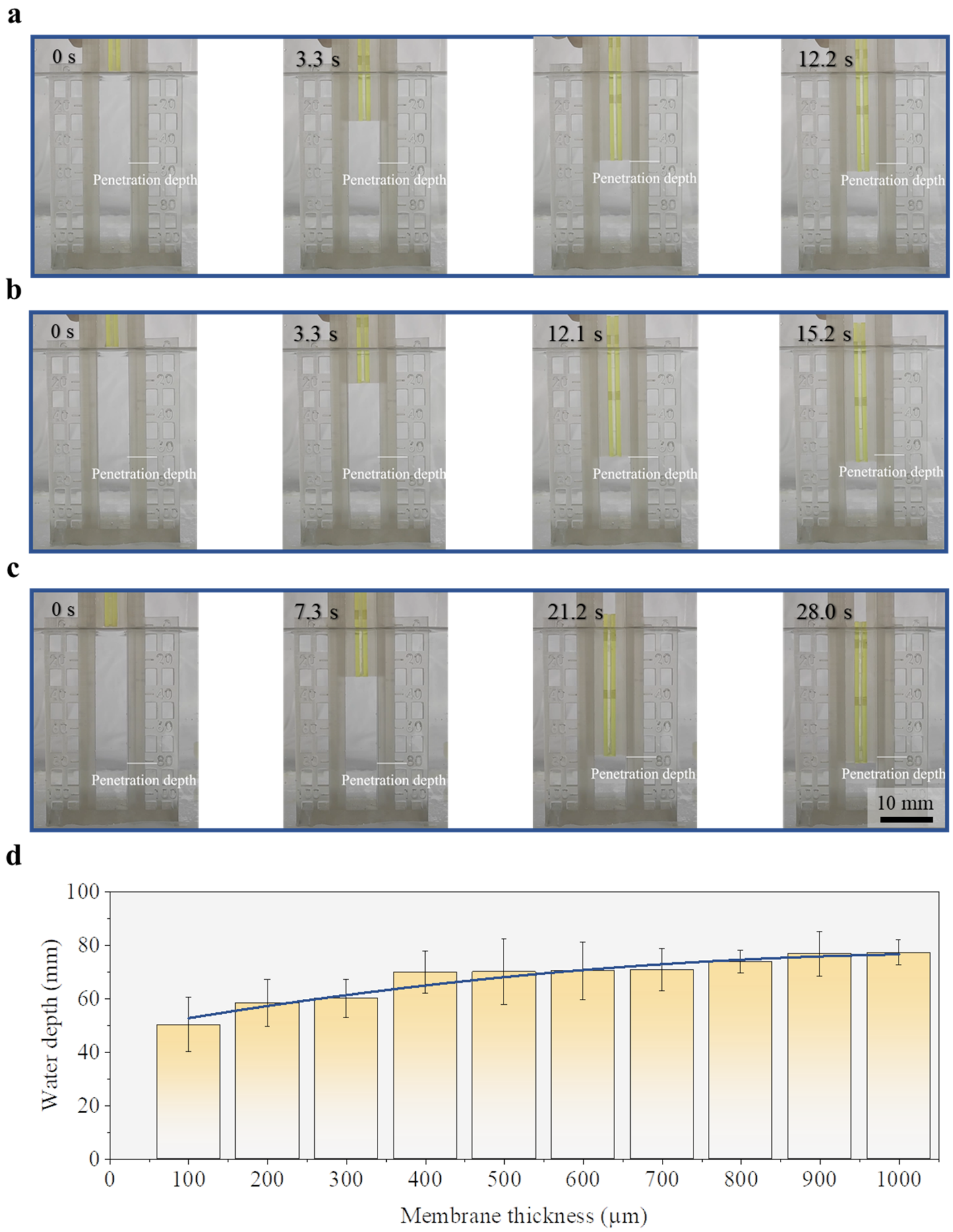

Figure S13. The influence of membrane thickness on the capability to withstand water depth. (a) When the membrane's thickness was 100 μm, the water depth the membrane could withstand was about 55 mm. (b) When the membrane's thickness was 600 μm, the water depth the membrane could withstand was about 65 mm. (c) When the membrane's thickness was 1000 μm, the water depth the membrane could withstand was about 75 mm. (d) As the membrane thickness increased, the depth of water it can withstand increased.

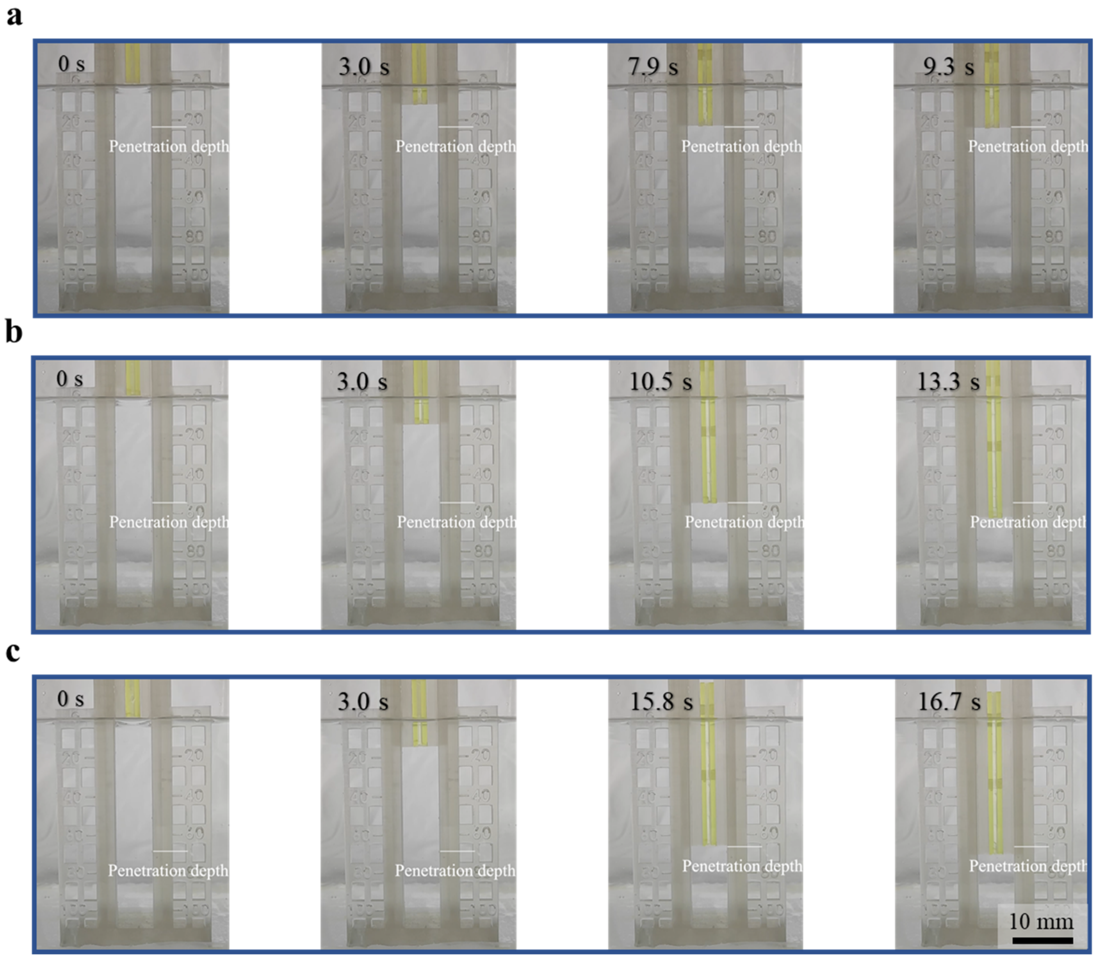

Figure S14. The influence of the distance between two adjacent holes on the capability to withstand water depth. (a) When the distance between two adjacent holes was 150 μm, the water depth the membrane could withstand was about 22 mm. (b) When the distance between two adjacent holes was 350 μm, the water depth the membrane could withstand was about 55 mm. (c) When the distance between two adjacent holes was 600 μm, the water depth the membrane could withstand was about 65 mm.

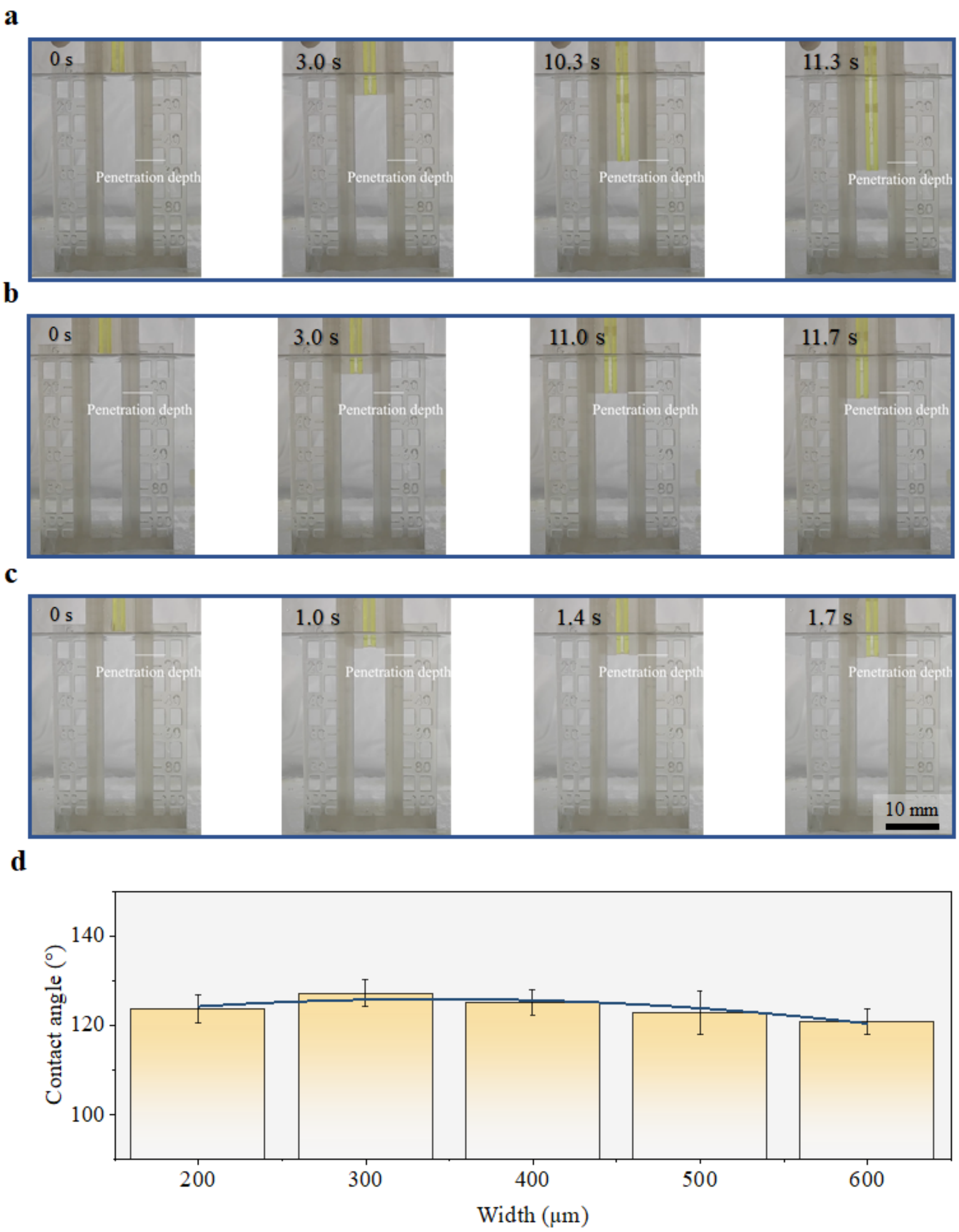

Figure S15. The influence of the hole's width on the capability to withstand water depth. (a) When the hole's width was 150 μm, the water depth the membrane could withstand was about 50 mm. (b) When the hole's width was 350 μm, the water depth the membrane could withstand was about 25 mm. (c) When the hole's width was 600 μm, the water depth the membrane could withstand was about 15 mm. (d) The contact angle of our bionic membrane increased with the hole's width before the hole's diameter reached 300 μm, and then decreased with the increase of hole's with afterwards.

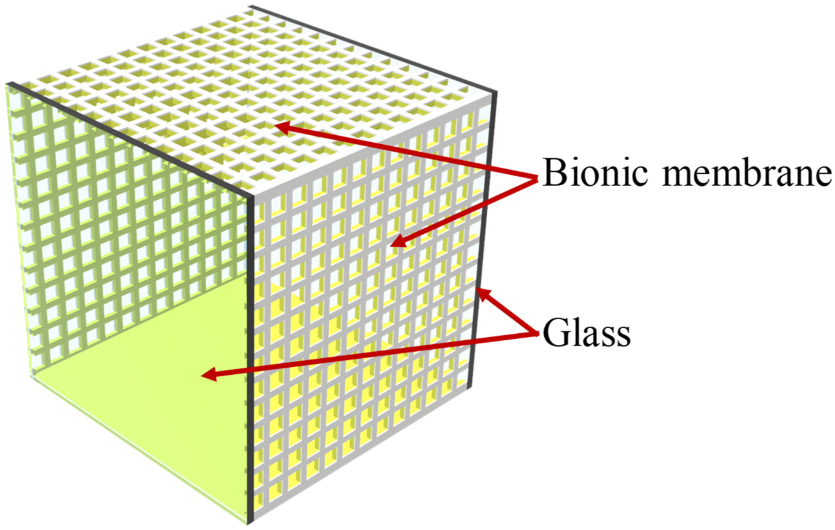

Figure S16. The schematic of cells used for the micro-reactor. The two membranes at the front and back of the cell were replaced with glass for the observation of the reactions inside of our bionic cells underwater.

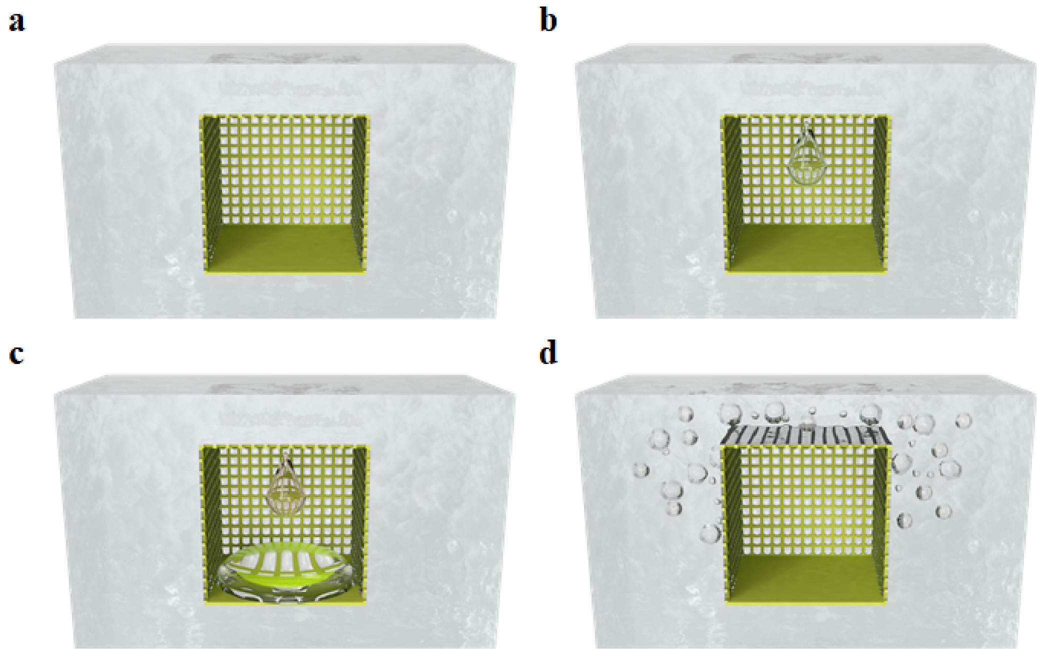

Figure S17. The schematic diagram of chemical reactions inside of the underwater bionic cell. (a) The bionic cell is underwater. (b) The first droplet was dripped on the platform inside of the open cell via a syringe needle. (c) Another droplet was dripped on the first droplet. (d) The reaction will take place after the coalescence of the two droplets.

Table S1. The detailed geometric parameters of our bionic cells.

Name of structure	Dimension
Overall length of the bionic cell	8.8 mm
Overall width of the bionic cell	8.8 mm
Overall height of the bionic cell	8.8 mm
Wall thickness of the bionic cell	400 μm
Width of the square hole	400 μm
Distance between two holes	200 μm

Table S2. The specific light-curing printing parameters for the fabrication of our bionic cell.

Name	Type
Material	Photosensitive resin
Light source	UV-LED (405 nm)
Exposure intensity	500 mw
Exposure time of the first layer	10 s
Printing thickness of a single layer	40 µm
Exposure time of a single layer	4 s

Supporting Movies include the following:

Movie S1 (.mp4 format). Unidirectional penetration in air.

Movie S2 (.mp4 format). Unidirectional penetration in underwater.

Movie S3 (.mp4 format). The influence of microholes' morphology on the capability to withstand water depth.

Movie S4 (.mp4 format). The influence of membrane's thickness on the capability to withstand water depth.

Movie S5 (.mp4 format). The influence of distance between two adjacent microholes on the capability to withstand water depth.

Movie S6 (.mp4 format). The influence of width of microholes on the capability to withstand water depth.

Movie S7 (.mp4 format). Generation of CO_2 under water.

Movie S8 (.mp4 format). The bionic cell spurts out liquid inside of the bionic cell.

Movie S9 (.mp4 format). Precipitation of $Fe(OH)_2$ under water.

Movie S10 (.mp4 format). Self-cleaning of $Cu(OH)_2$ precipitation underwater.